Matrix Photochemistry at Low Temperatures and Spectroscopic Properties of γ-Butyrothiolactone

Nahir Y. Dugarte,[†] Mauricio F. Erben,*,[†] Rosana M. Romano,[†] Mao-Fa Ge,[‡] Yao Li,[‡] and Carlos O. Della Védova*,[†,§]

CEQUINOR (UNLP-CONICET, CCT La Plata), Departamento de Química, Facultad de Ciencias Exactas, Universidad Nacional de La Plata, C.C. 962 (1900), La Plata, República Argentina, State Key Laboratory for Structural Chemistry of Unstable and Stable Species, Institute of Chemistry, Chinese Academy of Sciences, Beijing 100080, China, and LaSeISiC (CIC-UNLP-CONICET), Departamento de Química, Facultad de Ciencias Exactas, Universidad Nacional de La Plata, Camino Centenario y 508, Gonnet, República Argentina
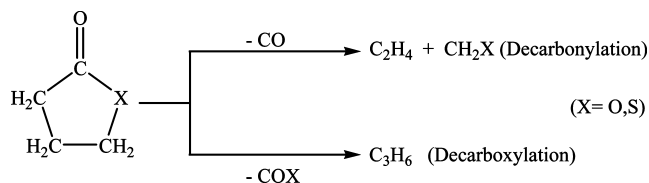
The five-membered heterocyclic γ-butyrothiolactone was isolated in a low-temperature, inert Ar matrix, and the UV−visible ($200 \leq \lambda \leq 800$ nm)-induced photochemistry was studied. On the basis of the IR spectra, the formation of ethylketene ($CH_3CH_2CH{=}C{=}O$) was identified as the main channel of photodecomposition. The valence electronic structure was investigated by He(I) photoelectron spectroscopy assisted by quantum chemical calculations at the outer valence Green's function/6-311++G(d,p) level of theory. The first three bands at 9.54, 9.69, and 11.89 eV are assigned to the n_S, n_O, and $\pi_{C=O}$ orbitals, respectively, denoting the importance of the −SC(O)− group in the outermost electronic properties. The conventional ring strain energy was determined to be 3.8 kcal mol^{-1} at the G2MP2 level of calculation within the hyperhomodesmotic model.

Introduction

The products formed in the thermal decomposition of lactones depend markedly on the size of the ring. Pyrolysis ($T \approx 520$ °C) of lactones of ring size larger than six atoms results in elimination, to yield an unsaturated acid.[1] In contrast, four-membered ring β-lactones decompose at lower temperatures (140−160 °C) into carbon dioxide and ethylene via a concerted pathway.[2,3] Little is known about the behavior of thiolactones, that is, the analogous species having a sulfur atom in the cycle. The unimolecular thermal decomposition of γ-butyrolactone and γ-butyrothiolactone has been studied in a flow system by using He I photoelectron spectroscopy and quantum chemical calculations.[4,5] For the sulfur-containing heterocycle, decarbonylation and decarboxylation pathways (see Scheme 1) are the main and minor decomposition channels, respectively.[4,5] Interestingly, the opposite trend is experimentally found for γ-butyrolactone.[6] Further theoretical studies for γ-butyrothiolactone showed that the calculated reaction profile for decarbonylation is favored over decarboxylation by 25.8 kJ mol^{-1}, within the UMP4/6-31G**//UHF/6-31G** approximation.[7] From a photoelectron spectroscopy (PES) study, it was indicated that little conjugative interaction between the carbonyl group and the sulfur atom is present, favoring the extrusion of CO over OCS in the thermal decomposition of γ-butyrothiolactone.[8]

The photodecomposition of isolated β-propiothiolactone, the four-member cyclic thiolactone, was recently studied in an Ar matrix.[9] On the basis of the interpretation of the infrared spectra after broad-band UV−vis irradiation, methylketene ($CH_3-HC{=}C{=}O$) is the main photoproduct, and thus, different pathways seem to be accessible when the molecule interacts with photons, as compared with the thermal route. For cyclic compounds it is well-known that the degree of strain energy parallels their reactivities.[10] This fact could be related to the changes observed in the product distribution when the size of the lactone rings varies. How these properties are related to and the ultimate affect the stability of thiolactones have not been elucidated so far.

In the present work, the photochemical study of thiolan-2-one (from now onward: γ-butyrothiolactone) isolated in an argon matrix is reported. The matrixes were irradiated with broad-band UV−visible ($200 \leq \lambda \leq 800$ nm), and the photoproducts were identified on the basis of the IR spectra of the matrixes. To investigate the effect caused by the electronic properties on the photochemical behavior, the gas-phase photoelectron spectra (PES) have also been obtained, and a comprehensive structural study was accomplished by applying quantum chemical calculations at the B3LYP and MP2 theories and employing 6-311++G(d,p) and aug-cc-pVTZ basis sets. The strain energy was determined within the s-homodesmotic model, including high-level MP2/6-311+G(2df,2pd) and G2MP2 methods.

SCHEME 1: Decarbonylation and Decarboxylation Pathways for Γ-Butyrolactone (X = O) and γ-Butyrothiolactone (X = S)

Experimental Section

γ-Butyrothiolactone (estimated purity >98%) was purchased from Aldrich and subsequently purified by repeated trap-to-trap distillation in vacuum. The final purity in both the vapor and

* To whom correspondence should be addressed: Phone/Fax: 54-221-425 9485. E-mails: (C.O.D.V.) carlosdv@quimica.unlp.edu.ar, (M.F.E.) erben@quimica.unlp.edu.ar.
   [†] CEQUINOR (UNLP-CONICET, CCT La Plata).
   [‡] Chinese Academy of Sciences.
   [§] SeISiC (CIC-UNLP-CONICET).

γ-Butyrothiolactone

J. Phys. Chem. A, Vol. 114, No. 35, 2010 **9463**

liquid phase was carefully checked by reference to the reported IR, CG/MS, and ^{1}H and ^{13}C NMR spectra.[11]

For the matrix experiments, the gas mixture of γ-butyrothiolactone with Ar was prepared in approximate compositions 1:500 by standard manometric methods. The mixture was deposited on a CsI window cooled to ∼15 K by a Displex closed-cycle refrigerator (SHI-APD Cryogenics, model DE-202) using the pulsed deposition technique. The IR spectrum of the matrix sample was recorded at a resolution of 0.5 cm^{-1} and with 256 scans using a Nexus Nicolet instrument equipped with either an MCTB or a DTGS detector (for the ranges 4000−400 or 600−250 cm^{-1}, respectively). Following deposition and IR analysis of the resulting matrix, the sample was exposed to broad-band UV−visible radiation (200 ≤ λ ≤ 800 nm) from a Spectral Energy Hg−Xe arc lamp operating at 800 W. The output from the lamp was limited by a water filter to absorb infrared radiation and so minimize any heating effects. The IR spectrum of the matrix was then recorded at different times of irradiation to analyze closely the decay and growth of the various absorptions.

The PE spectrum was recorded on a double-chamber UPS-II machine, which was designed specifically to detect transient species, as described elsewhere,[12,13] at a resolution of ∼30 meV, indicated by the standard Ar$^+$(^{2}P$_{3/2}$) photoelectron band. Experimental vertical ionization energies were calibrated by simultaneous addition of a small amount of argon and methyl iodide to the sample.

Quantum chemical calculations were performed using program package Gaussian 03.[14] Full geometry optimization was performed by applying ab initio (MP2) and DFT (B3LYP) methods using the 6-311++G** and aug-cc-pVTZ basis set. The calculated vibrational properties correspond in all cases to potential energy minima for which no imaginary frequencies are found. The vertical ionization energies (E_v) were calculated according to Cederbaum's outer valence Green's function (OVGF) method[15,16] with the 6-311++G(d,p) basis set based on the B3LYP/6-311++G(d,p) optimized geometry. The Mulliken population analysis was applied for assigning charges for both neutral and radical-cationic forms.

The strain energy of the title compound has been calculated by applying the s-homodesmotic approach introduced by Zhao and Gimarc.[17] To obtain the energies for all acyclic systems, optimum equilibrium geometries were computed for the singlet ground states of all pertinent molecular systems using B3LYP and MP2 methods with the 6-311++G(d,p) basis set. Several conformations were computed to achieve the lowest energy conformation for each molecular system. For each conformation, harmonic vibrational frequencies were also calculated at the same level of computation to ensure that each optimized geometry corresponds to a true local minimum and to obtain the zero-point energy correction. In all cases, electronic energies plus the zero-point energy were used to compute the strain energies. Additionally, following the recommendation reported by Ringer and Magers,[18] electronic energies of the resulting minima were recalculated using single-point energy calculations at the MP2/6-311+ G(2df,2pd) level. Finally, the strain energy was obtained with the high-level composite method G2MP2.[19,20]

Result and Discussions

Molecular Structure. From the spectroscopic studies reported by Alonso and co-workers, it is well-known that a nonplanar ring adopting a twisted conformation is expected for γ-butyrothiolactone.[21,22] The ground state rotational constants
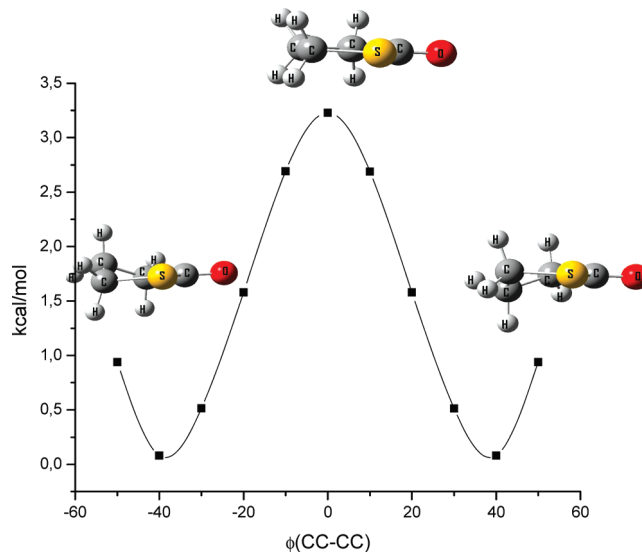

Figure 1. Potential energy curve of γ-butyrothiolactone for φ(CC−CC) dihedral angles around the minimum computed at the B3LYP/6-31G* level of approximation.

have been determined by microwave spectroscopy [A = 4448.784(0.004), B = 3143.310(0.004), and C = 1948.570(0.004) MHz], together with the dipole moment, with a value of $μ_{total}$= 4.268(0.023) D.[18] Moreover, the barrier for ring inversion through a planar ring structure was estimated to be 1380(350) cm^{-1} [3.9 (1.0) kcal mol^{-1}].

Theoretical calculations at the B3LYP/aug-cc-pVTZ and MP2/6-311++G(d,p) level of approximations have been applied to obtain a more detailed description of the molecular structure of the title species. In a first step, the potential energy curve for small variation of the φ(CC−CC) dihedral angle around the equilibrium value was obtained. This curve reproduces closely that obtained by Alonso et al. for the potential curve of the ring twisting vibration.[21,22] Two nonplanar enantiomeric structures were obtained, and the parameter typically used for describing these twisted conformation, the $τ_e$ angle, was computed to be ∼24 degrees, in very good agreement with the angle determined by microwave spectroscopy of 27 ± 7°.[22,23] In addition, the rotational constants and dipolar moments are well-reproduced by quantum chemical calculations, as compared in Table S1 in the Supporting Information. Other molecular parameters, including bond lengths and bond angles, are shown in Table S1 for different levels of approximations.
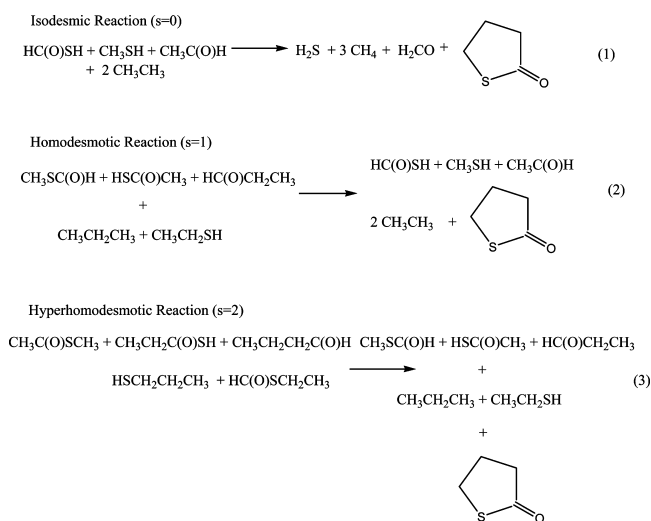
The two enantiomeric structures are connected by a ring inversion barrier characterized by possessing a planar structure of the ring atoms with C_s symmetry. In effect, the structure of the maximum corresponds to a transition state as characterized by the frequency calculation; that is, only one imaginary frequency was computed at 205i cm^{-1} [MP2/6-311++G(d,p)], corresponding to the ring twisting vibration. The calculated height barriers are 2.80, 4.32, and 3.59 kcal mol^{-1}, at the B3LYP/aug-cc-pVTZ, MP2/6-311++G(d,p), and G2MP2 levels of approximations, respectively. The latter value is in close agreement with the experimental result (see Figure 1).

Strain Energy. The strain energy of a molecule always entails a comparison between the molecule of interest and some term of reference, presumably strainless species.[24] For estimating the strain energy of γ-butyrothiolactone, high-level quantum chemical calculations have been applied within the s-homodesmotic

TABLE 1: Strain Energies (kcal mol^{-1}) for γ-Butyrothiolactone Determined within the Hyperhomodesmotic Model Using B3LYP, MP2, and G2MP2 Levels of Approximation

	B3LYP	MP2		
model	6-311++G**	6-311++G**	6-311+G (2df,2pd)	G2MP2
isodesmic	−7.82	−13.60	−14.40	−12.03
homodesmotic	1.92	2.91	3.21	2.63
hyperhomodesmotic	1.74	4.28	4.35	3.84

approach.[17,18] Equations 1−3 give the appropriate reactions needed for the title species.

Isodesmic Reaction (s=0)

$$HC(O)SH + CH_3SH + CH_3C(O)H \longrightarrow H_2S + 3 CH_4 + H_2CO + \text{(ring)} + 2 CH_3CH_3 \quad (1)$$

Homodesmotic Reaction (s=1)

$$CH_3SC(O)H + HSC(O)CH_3 + HC(O)CH_2CH_3 + CH_3CH_2CH_3 + CH_3CH_2SH \longrightarrow HC(O)SH + CH_3SH + CH_3C(O)H + 2 CH_3CH_3 + \text{(ring)} \quad (2)$$

Hyperhomodesmotic Reaction (s=2)

$$CH_3C(O)SCH_3 + CH_3CH_2C(O)SH + CH_3CH_2CH_2C(O)H + HSCH_2CH_2CH_3 + HC(O)SCH_2CH_3 \longrightarrow CH_3SC(O)H + HSC(O)CH_3 + HC(O)CH_2CH_3 + CH_3CH_2CH_3 + CH_3CH_2SH + \text{(ring)} \quad (3)$$

The conventional strain energies determined with the B3LYP and MP2 methods, including zero-point corrections, are listed in Table 1, together with the energy determined using G2MP2 method, to evaluate very accurate energies. From these results, it is apparent that the isodesmic model results in unreliable values, and the B3LYP method computes strain energy values that are moderately low, as compared with the MP2 method with identical basis sets. Homodesmotic reactions yield lower values than the hyperhomodesmotic model, denoting thus that high levels of "s" are required in the reaction scheme for a proper description of thiolactones. Moreover, with a triple-ζ quality basis set, the MP2 level showed little difference between the strain energy values obtained with the 6-311++G(d,p) and the more extended 6-311++G(2dp,2df) basis sets.[18] Thus, the MP2 average values of 4.31 kcal mol^{-1} for the hyperhomodesmotic method is in reasonable agreement with the strain energy of 3.84 kcal mol^{-1} calculated at the G2MP2 level of approximation within the same reaction scheme. These values are significantly lower than those obtained for β-propiothiolactone,[9] which are 16.9 and 16.4 kcal mol^{-1} at the same levels of calculations, respectively.

As analyzed recently by Bach and Dmitrenko,[25] the strain energy (SE) of a cyclic molecule is affected by the presence of functional groups or heteroatoms. For example the experimental SE of cyclopentane, the basic molecule for a five-membered cyclic species, is 6.2 kcal mol^{-1}.[26] Several studies have been reported for the corresponding cyclopentene,[27] cyclopentyne, and 1,2-cyclopentadiene.[28] A very high value of 84 kcal mol^{-1} has been reported for the elusive 1,2,3-cyclopentatriene molecule.[29] However, when a carbonyl group is introduced in the cyclopentane ring forming cyclopentanone, a low influence on

the SE is noted, with calculated values of 6.8 kcal mol^{-1} (CBS-Q). On the other hand, the replacement of a methylene group by an oxygen atom tends to increase the SE of the substituted ring; thereby, the computed strain energy for γ-butyrolactone is 8.2 kcal mol^{-1} (CBS-Q).[25] However, when the methylene group is formally replaced by a divalent sulfur atom, the SE value becomes lower.[30]

This tendency is also observed for γ-butyrothiolactone, with a calculated G2MP2 value of 3.84 kcal mol^{-1}, a SE definitively lower than the result computed at the same level for the reference cyclic species cyclopentane (6.61 kcal mol^{-1}).[31] Thus, the trend for the strain energy of five-membered molecules related with the title species is 1,2,3-cyclopentatriene >1,2-cyclopentadiene ≫ γ-butyrolactone > cyclopentanone ≈ cyclopentane > γ-butyrothiolactone.

Is well-known that the tension in cyclic molecules decreases as the size of the ring increases, affecting significantly both its molecular structure and chemical reactivity.[32] Such a trend can be rationalized on the basis of bond elongations or bond and torsion angle deformation phenomena arising when a cyclic molecule is formed, as compared with an idealized nonconstrained analog.[33] Accordingly, it is interesting to analyze the geometrical parameters of related species with different degrees of strain. Taking in account the previous work for β-propiothiolactone and the good correlation between calculated MP2/6-311++G** and experimental values, geometrical parameters for the title species obtained with the same method are discussed below. For example, the ∠C−S−C bond angle in β-propio-[9] and γ-butyrothiolactone are 77.27(5)° (X-ray) and 92.9° (MP2/6-311++G**), respectively. On the other hand, the bond angle values around the carbonyl group are higher in β-propiothiolactone[9] than in γ-butyrothiolactone: ∠O=C−S and ∠O=C−C amount to 131.25(9)° and 134.20(11)°, respectively for β-propiothiolactone, whereas in γ-butyrothiolactone, the computed values are 123.7 and 126.2 degrees, respectively. The value of the associated endocyclic ∠C2−C1−S bond angle in γ-butyrothiolactone is 110.1°, significantly lower than the ideal value of 120° expected for an sp^2-hybridized carbon atom. Even lower is the value reported for the strained β-propiothiolactone, which is 94.55(7)°.[9]

A comparison of geometrical parameters between thiolactones and the corresponding acyclic species is also of interest. It should be noted that acyclic thioesters result in a structure with synperiplanar conformation (C=O double bond syn with respect to the S−Y single bond in a XC(O)SY molecule).[34−37] In contrast, short-chained cyclic thiolactones are forced to adopt an antiperiplanar conformation. In effect, remarkable differences between bond angles of the title species with the associated acyclic thioesters [the isomeric S-methyl thiopropionate, CH$_3$SC(O)CH$_2$CH$_3$, and S-ethyl thioacetate, CH$_3$CH$_2$SC(O)CH$_3$, molecules] are observed. The computed (MP2/6-311++G**) values for the ∠O=C−S and ∠O=C−C bond angles are 122.7, 123.2 [CH$_3$SC(O)CH$_2$CH$_3$], and 122.4 and 124.1 degrees [CH$_3$CH$_2$SC(O)CH$_3$], respectively.

HeI Photoelectron Spectra. Differences in the physicochemical behavior, especially for photoinduced processes, between oxo- and thiolactones are expected because differences in the electronic properties of the central −C(O)X− (X = O, S) moiety exist. In effect, the valence electronic properties of the γ-butyrolactone (X = O) are well-known,[38] and the HOMO and HOMO-1 correspond to nonbonded orbitals formally located on the oxygen atoms of the carbonyl and ester groups, respectively.[39] On the other hand, Chin et al.[8] reported the HeI and HeII photoelectron spectra of γ-butyrothiolactone (X = S)
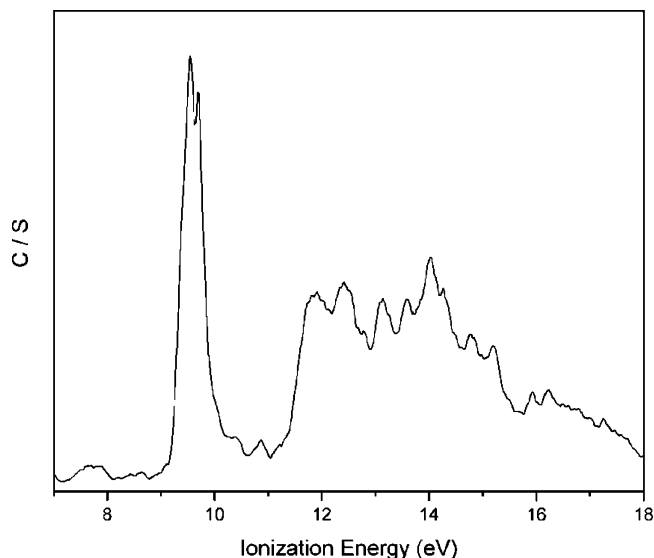
γ-Butyrothiolactone

J. Phys. Chem. A, Vol. 114, No. 35, 2010 **9465**

Figure 2. He(I) photoelectron spectrum of γ-butyrothiolactone.

Figure 3. Correlation diagram of the ionization potentials of methylthioacetate,[40] β-propiothiolactone,[9] γ-butyrothiolactone, and S-ethyl thioacetate.[42] The characters for the three outermost molecular orbitals of γ-butyrothiolactone are also shown.

TABLE 2: Experimental Vertical Ionization Energies (IP in eV), Computed Ionization Energies (E_v in eV) at the OVGF/6-311++G(d,p) Level of Approximation and Molecular Orbital Characters for γ-Butyrothiolactone

IP (eV)	E_v (eV)[a]	MO	character
9.54	9.18	(27)	$n_{S(\pi)}$
9.69	9.72	(26)	n_O
11.89	11.66	(25)	π_{CO}
12.41	12.58	(24, 23)	σ_{C3-H}
13.60	13.78		
13.13	13.10	(22, 21)	σ_{C2-H}
14.05	14.36		
14.28	14.62	(20, 19)	σ_{C4-H}
14.79	15.00		
	16.24	(18)	σ_{C4-S}

[a] Molecular geometry optimized at the B3LYP/6-311++G(d,p) level.

and assigned the signal assisted by a semiempirical PM3 and HF/6-31G* calculations. The proposed assignment indicates that the four first bands at 9.49, 9.66, 11.80, and 12.29 eV are mainly related to ionizations from n_S (HOMO), n_O, $n_S(\sigma) + \sigma_{C-S}$, and $\pi_{C=O}, +, \pi_{CH_3}$ orbitals, respectively. This sequence for the outermost orbitals, however, is slightly different from that reported for other −SC(O)−containing species.[9,12,40−42] In effect, the third band is usually assigned to the electron ejection from the $\pi_{C=O}$ orbital. Both $n_S(\sigma)$ and σ_{C-S} are lower in energy, with IP higher than 15 eV. To clarify this discrepancy is of interest, since molecular orbitals formally located on the central −SC(O)− group, the main chromophore of γ-butyrothiolactone, are involved. Thus, we decide to remeasure the HeI photoelectron spectrum with improved resolution and to complement the band assignment with the assistance of the higher-level quantum chemical calculations based on the OVGF, beyond that of a single determinant wave function.

The PE spectrum of γ-butyrothiolactone is presented in Figure 2; the general features are similar to those reported previously.[8] The experimental ionization energies (IP in eV), calculated vertical ionization energies at OVGF/6-311++G(d,p) (E_v in eV), and molecular characters are summarized in Table 2.

Two bands appear in the energy range between 9 and 10 eV, and after a relatively large gap, a group of overlapping bands are present between 11.5 and 18 eV. The first two bands show narrow, sharp contours, suggesting a relative nonbonding
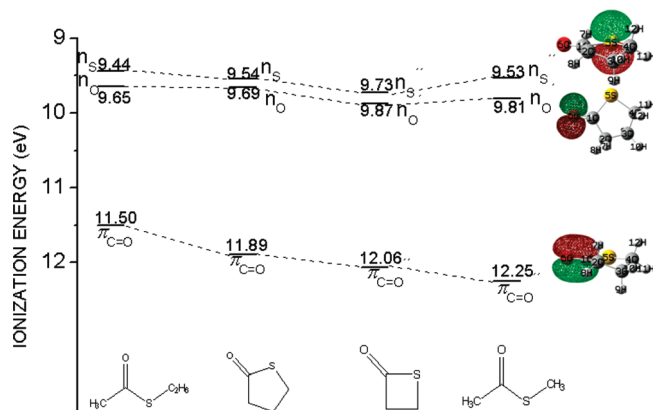
character, which can be attributed to ionization processes from both sulfur and oxygen lone-pair electrons (n_S, n_O) of the −SC(O)− group, respectively, as assigned already by Chin et al.[8] As commented, the third band appearing at 11.89 eV had been assigned in the previously work[8] to the ionization of the $n_S(\sigma)$ orbital with a significant σ_{C-S} contribution. Our quantum chemical calculations predict that this band is associated with an ionization process from the $\pi_{C=O}$ orbital, the vertical ionization energy for the $n_S(\sigma)$ orbital being ultimately higher, with a calculated value of 16.24 eV. A group of overlapping bands between 13 and 16 eV can be originated by ionizations from the σ_{CH_2} orbitals, as predicted by the OVGF calculations.

It has been proved that the comparison of the PE spectra for a series of related compounds is useful for the assignment of their bands.[43] Such a correlation diagram between the first three IPs of γ-butyrothiolactone and those of the related species S-ethyl thioacetate,[42] S-methyl thioacetate[40] and β-propiothiolactone[9] is drawn in Figure 3. The three outermost orbitals are less stabilized in the five- than in the four-membered thiolactone. The major change in the ionization energy observed for this series is related with the $\pi_{C=O}$ orbital, which is more stabilized in S-methyl thioacetate (12.25 eV)[40] and β-propiothiolactone (12.06 eV).[9] Previous natural bond orbital calculations for these species computed quite similar donor−acceptor properties for the $\pi_{C=O}$ orbital.[9] Inductive electron donating properties of the alkylated chain could play an important role in the orbital stabilization.

Further calculations at the UB3LYP/6-311++G** level of approximation were performed to analyze the nature of the cation formed in the first ionization process. The results demonstrate that the atomic charges are delocalized all over the low-lying radical cation, with an appreciable fraction localized at the −C(O)S− group, as is evident from Table S3 (Supporting Information). The cyclic nonplanar molecular geometry (C_1 point group) is retained after the ionization with a C1−S bond elongation of 0.36 Å in the fundamental cationic state, the bond angles being almost the same in both species. Therefore, similar Franck−Condon factors can be anticipated for the neutral molecule and the low-lying cation. As expected, the first ionization observed in the photoelectron spectrum results in a narrow and structureless band.

Vibrational Analysis. Since we are interested in the photochemical behavior of matrix-isolated γ-butyrothiolactone using tools derived from the vibrational spectroscopy, an unambiguous study of its vibrational properties is necessary. Consequently,
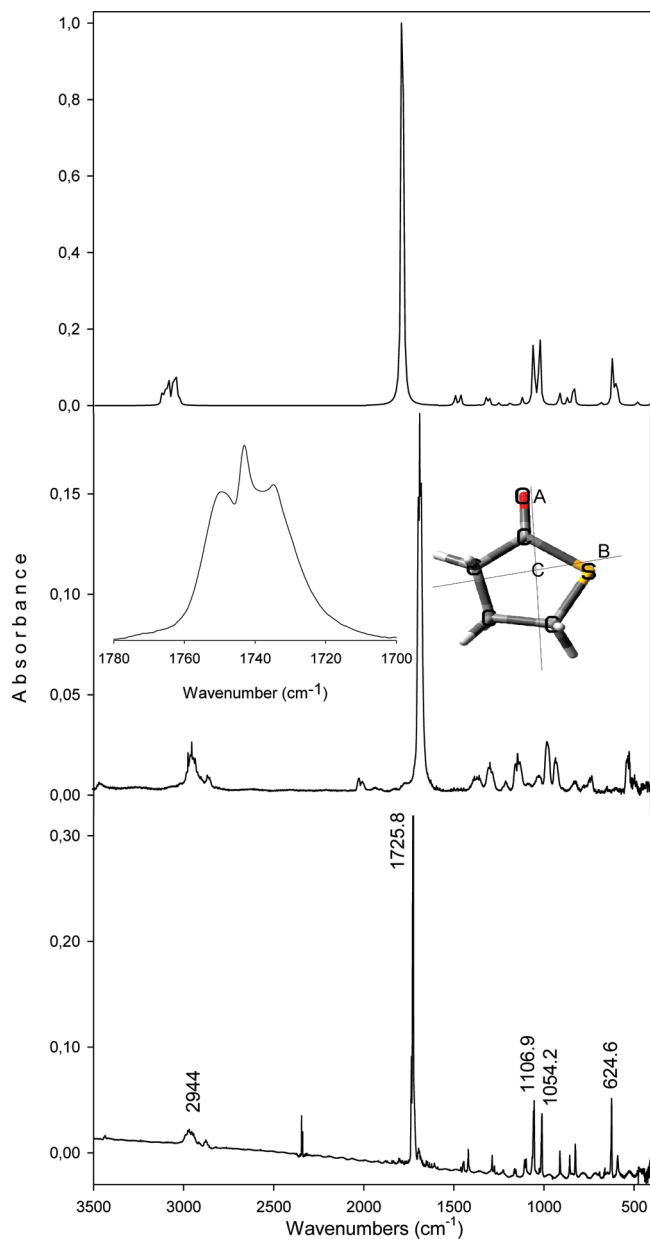
Figure 4. (top) Calculated vibrational spectrum at the B3LYP/aug-cc-pVTZ level of approximation. (middle) Gas IR spectrum at 0.7 mbar (glass cell, 200 mm optical path length, Si windows, 0.5 mm thick). (bottom) FTIR spectrum of an Ar matrix γ-butyrothiolactone following sample deposition. An enlargement of the νC=O stretching mode region is shown in the inset figure together with principal moments of inertia (A and B in the sheet plane).

the gas and liquid phase infrared as well as the Raman (liquid) spectra for the title species have been measured and compared with available data[11,44] (Figure 1 in the Supporting Information). Moreover, for a more detailed vibrational study, the Ar-matrix-isolated spectrum was also measured. Results obtained from the theoretical calculations were used to tentatively assign the bands observed in the vibrational spectra. The experimental (gas phase and argon matrix IR) and calculated (B3LYP/aug-cc-pVTZ) vibrational spectra are compared in Figure 4, showing a good correspondence. The experimental and calculated frequencies are shown in Table 3.

The most intense IR band corresponds to the C=O vibration, which possesses a well-defined rotational contour corresponding to an A-type band, with a P−R separation of 15 cm^{-1} (see Table 3). This feature is in agreement with the almost parallel

orientation of the carbonyl oscillator expected for the ν(C=O) normal mode (dipole derivative vector) with respect to the principal axis of inertia, A. Figure 4 shows an enlargement of the ν(C=O) zone and the main inertial axes of γ-butyrothio-lactone. Following the classical procedure proposed by Seth-Paul,[45] a semiquantitative analysis of the band contours has been performed.[46] The title molecule belongs to the C_1 symmetry point group and can be classified as a prolate asymmetric rotors, with an asymmetric parameter $\kappa_{exp} = -0.044\ 289$ as calculated from the transitions observed in the microwave spectrum[18] [$\kappa_{calc} = -0.044\ 58$ at the MP2/6-311++G(2df,2pd) level]. Thus, from its rotational constants, the calculated PR separations expected for A, B, and C type bands are 15.7, 11.6, and 23.5 cm^{-1}, respectively, in good agreement with the observed values (see Table 3).

The infrared spectrum of γ-butyrothiolactone isolated in an Ar matrix allows a more detailed assignment of the bands. In Table 3, the integrated absorptions of the matrix bands are also listed, showing a very good correlation between the experimental and the calculated intensities. It is important to note that several bands in the Ar-matrix spectrum are split, possibly due to matrix-cage effects.

UV−Visible-Induced Photochemistry in Low-Temperature Inert Matrixes. After deposition, the γ-butyrothiolactone/Ar matrix was exposed to broadband UV−visible radiation (200 $\leq \lambda \leq$ 800 nm) for different irradiation times ranging from 10 to 900 s, and the IR spectrum was measured at each stage. Figure 5 shows the 1755−1710 cm^{-1} carbonyl region, illustrating that after 900 s of broadband UV−visible irradiation, almost all initial γ-butyrothiolactone was consumed. Table 4 lists the wavenumbers of all of the IR absorptions that develop upon photolysis. To distinguish the bands corresponding to the different species and to determine the sequence of the changes, the integrated intensities of the new bands have been plotted as a function of irradiation time.

By far, the most intense of these new bands occurs at ~2130 cm^{-1} (see Figure 6), where a rather broad absorption is observed. This band shows a complex feature, with several narrow peaks appearing superposed, with maxima at 2143.7, 2137.1, 2135.4, 2131.2, 2126.6, and 2122.0 cm^{-1}. These features are retained without variations along the different irradiation stages, as observed in Figure 6 and Figure S2 in the Supporting Information.

At this point, it is of central significance to distinguish whether this band originates from either carbon monoxide or a ketene molecule. The distinction between these species by using infrared spectroscopy is a nontrivial problem because both $\nu(^{12}C=O)$ fundamentals are expected as very intense absorption, with remarkably similar frequency values. To distinguish between them, the analysis of the satellite absorptions corresponding to $\nu(^{13}C=O)$ has previously been proposed.[47] In the spectra of irradiated γ-butyrothiolactone, a satellite band at 2073.4 cm^{-1} is observed, with an intensity ratio roughly close to 1% of the intense bands at around 2131 cm^{-1}. Such a low frequency value for a $\nu(^{13}C=O)$ fundamental suggests that a ketene molecule is formed predominantly. In principle, three different ketene species (i.e. ketene ($H_2C=C=O$), methylketene ($CH_3CH=C=O$), and ethylketene ($CH_3CH_2CH=C=O$)) could be formed from the title molecule. To distinguish between the formation of specific ketene molecules, a detailed comparison between the argon matrix spectra reported for $H_2C=C=O$,[48] $CH_3CH=C=O$,[49] and $CH_3CH_2CH=C=O$[50] has been performed. It should be noted that the reported spectrum available in the literature for ethylketene comes from the photolysis of cro-

TABLE 3: Experimental Liquid-, Gas-Phase, Ar-Matrix Infrared Spectra, Raman Spectra (liquid) and Calculated Vibrational Frequencies (cm⁻¹) of γ-Butyrothiolactone

	experimental			B3LYP/Aug-cc-pVTZ		
FTIR (liquid)	FTIR (gas)	FT-Raman (liquid)	Ar matrix (I %)	ν [cm⁻¹]	$I_{IR}{}^{a}$	tentative assignment
			3435.6 (3)			$2\nu CO$
	2987		2989	3116.8	(2)	$\nu_{as}CH_2$
2965	2974 R	2968	2972 broad	3102. 4	(2)	$\nu_{as}CH_2$
	2967 Q		2953			
	2957 P					
2937	2947	2942	2944 (2)	3083.9	(5)	$\nu_{as}CH_2$
2902	2916	2900	2916.1 (1)	3056.6	(4)	$\nu_{s}CH_2$
2868	2883 R	2871	2877.2 (6)	3043.8	(6)	$\nu_{s}CH_2$
	2878 Q					
	2870 P					
2804		2810	2822 (<1)	3024.7	(1)	$\nu_{s}CH_2$
1773sh	1750 R	1702	1727.4 (100)	1785.5	(100)	νCO
1704	1743 Q		1725.8			
	1735 P					
1439	1434	1441	1460.9 (<1)	1501.7	(<1)	δCH_2
1408		1411	1449.1 (2)	1489.8	(1)	δCH_2
			1444.9			
1388			1419.6 (4)	1462.1	(2)	δCH_2
1364	1372 R	1324	1287.9 (3)	1361.8	(<1)	δCH_2 wagging
	1365 Q					
	1354 P					
	1280	1288	1274.9 (1)	1319.3	(1)	δCH_2 wagging
1273		1273	1261.9 (1)	1303.0	(1)	δCH_2 wagging
1259						
1221	1228 R	1223	1227.1 (1)	1251.1	(<1)	CH_2 twisting
	1217 Q		1223.8			
	1205 P					
1161		1163	1162.5 (3)	1186.1	(<1)	CH_2 twisting
			1156.3			
1101	1106	1101	1106.9 (7)	1118.9	(1)	CH_2 twisting
	1100		1098.6			
1058	1059	1056	1057.6 (22)	1057.2	(11)	$\nu C1-C2$
			1054.2			
			1026.2 (1)	1030.6	(<1)	ρCH_2
1010	1013	1014	1011.9 (11)	1022.9	(12)	$\nu_{as}C4-C3-C2$
			1010.6			
908	913	910	911.3 (5)	912.7	(2)	$\nu_{s}C4-C3-C2$
	904					
853	830	856	857.1 (4)	868.7	(1)	ρCH_2
824	818					
728	736	825	826.1 (5)	834.4	(4)	ρCH_2
685		687	691.4 (1)	683.6	(<1)	νCH_2-S
628	618	632	624.6 (12)	618.0	(8)	$\nu S-C(O)$
			623.5			
590		591	590.7 (9)	595.7	(5)	$\delta CC(O)S$
				483.6	(<1)	$\delta oop(C=O)$
475		478		475.4	(<1)	$\delta \, CH_2SC$
		404		398.9	(1)	ρCO
		230		223.3	(<1)	τ
				130.6	(<1)	τ

a Intensities in parentheses normalized relative to that of the most intense band set equal to 100% = 424 Km/mol.

tonaldehyde in an Ar matrix, and only the most intense absorption was reported.[50] Several other features that might be in principle assigned to these species become apparent in the product spectra of the title compound.

Frequency calculations at the B3LYP/aug-cc-pVTZ level of approximation for these three ketenes have been performed to assist the analysis of the postphotolysis infrared spectra. The corresponding computed frequency values and intensities are given as Supporting Information. In particular, quantum chemical calculations compute a diminution in the frequency of the $\nu(C=O)$ mode in the ketene moiety with alkylation. The computed values in the series $RHC=C=O$, with R = H, CH_3, and CH_2CH_3, are 2211, 2197, and 2193 cm⁻¹, respectively, and the computed shift expected for the $\nu(^{13}C=O)$ mode is the same for all the three species, 11 cm⁻¹. Thus, the feature observed for the $\nu(^{13}C=O)$ fundamental in the photolysis of the title

species at 2073.4 cm⁻¹ appears at slightly but definitively lower wavenumbers than that of ketene (2080.4 cm⁻¹)[47] and methylketene (2075.3 cm⁻¹).[9] Thus, taking into account not only the strong absorptions near 2131.2 cm⁻¹ and its satellite at 2073.4 cm⁻¹, but also absorptions at 1410.3 and 1338.7 cm⁻¹ that appeared after irradiation of the matrix, we are led to conclude that a major product is the ethylketene molecule, CH_3CH_2-$HC=C=O$. The integrated intensities of these bands as a function of the irradiation time had shown a similar profile, growing continuously with the photolysis, as depicted in Figure 7.

A moderately strong band associated with the out-of-plane type bending mode vibration [$\delta(C-H)$] is expected for ketene species in the 600−500 cm⁻¹ region. The infrared spectra of photolyzed γ-butyrothiolactone show the development of a band at 541.5 cm⁻¹, which is also in reasonable agreement with the
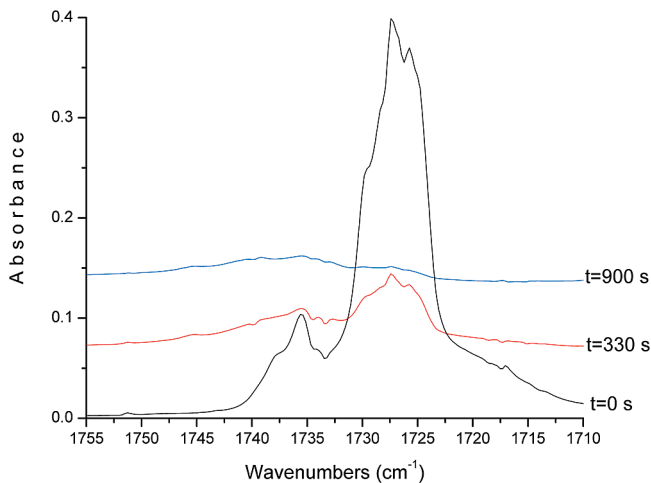
Figure 5. FTIR spectrum for an Ar matrix initially containing γ-butyrothiolactone at different irradiation times in the region of 1755−1710 cm^{-1}.
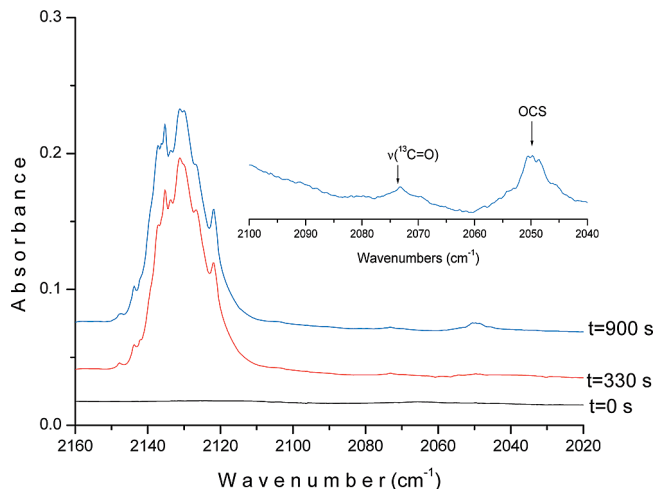

Figure 6. FTIR spectrum for an Ar matrix initially containing γ-butyrothiolactone at different irradiation times in the regions of 2160−2020 cm^{-1}.

B3LYP/aug-cc-pVTZ computed value for ethylketene (581 cm^{-1}). On the basis of quantum chemical calculations, other less intense bands can be tentatively also assigned to the ethylketene molecule (see Table 4 for the proposed assignment).

Minor quantities of thioformaldehyde, $H_2C=S$, are also likely to be formed. Indeed, even at very short irradiation times, a structured absorption at ∼995 cm^{-1} can be observed.[51] This band grows continuously with the irradiation time, as observed in Figure 7. However, an unambiguous identification for thioformaldehyde cannot be done because near 1050 cm^{-1}, where a second band is expected for $H_2C=S$, the γ-butyrothiolactone species strongly absorbs (see Table 4), precluding a more detailed analysis of the matrix infrared spectra.

Finally, a third photodissociation channel is opened at longer irradiation times. Thus, after 330 s of UV−vis irradiation, the presence of a moderately intense band at 2049.9 cm^{-1} denotes the formation of OCS, as can be observed in Figure 6. At this point, the dissociation channels responsible for the formation of minor quantities of these molecules remain obscure.

Conclusion

The methylketene species $CH_3CH_2HC=C=O$ is formed predominantly in the photochemically induced decomposition of UV−vis irradiated γ-butyrothiolactone isolated in an Ar matrix. This behavior contrasts with the thermal dissociation

TABLE 4: Wavenumbers, Intensities and Assignments of the IR Absorptions Appearing after 900 s of Broadband Photolysis of γ-Butyrothiolactone Isolated in an Ar Matrix

matrix FTIR		assignment		wavenumber reported previously/calcd value[a]
ν [cm^{-1}]	I	molecule	vibrational mode	
3502.1	0.02	$CH_3CH_2HC=C=O$	$\nu(C=O) + \delta(CH_3)$	$2131.2 + 1410.3 = 3541.5$
3074.3	0.01	$CH_3CH_2HC=C=O$	$\nu(C-H)$	3172
2964.0	0.02	$CH_3CH_2HC=C=O$	$\nu(CH_3)$	2966[52]
2940.3	0.01	$CH_3CH_2HC=C=O$	$\nu(CH_3)$	3095
				3086
2864.1	0.03	$CH_3CH_2HC=C=O$	$\nu_{as}(CH_2)$	3058
				3015
2135.4[b]	0.72	$CH_3CH_2HC=C=O$	$\nu(C=O)$	2124[50]
2131.2[b]	0.75			
2073.4	<0.01	$CH_3CH_2HC=C=O$	$\nu(^{13}C=O)$	
2049.9	0.04	OCS	$\nu(C=O)$	2049.6[53,54]
1449.4	<0.01	$CH_3CH_2HC=C=O$	$\delta_{as}(CH_3)$	1505
1439.1	0.02	$CH_3CH_2HC=C=O$	$\delta_s(CH_3)$	1496
1410.3	0.02	$CH_3CH_2HC=C=O$	$\delta_{as}(CH_2)$	1428
1391.1	<0.01	$CH_3CH_2HC=C=O$	$\nu(C=C)$	1411
1338.7	0.02	$CH_3CH_2HC=C=O$	$\delta_s(CH_2)$	1348
1140.7	0.06	$CH_3CH_2HC=C=O$	$\nu(C-C)$	1160
1061.7	<0.01	$CH_3CH_2HC=C=O$	$\nu(C-C)$	1086
1044.6	<0.01	$CH_3CH_2HC=C=O$	$\delta oop(CH_2)$	1106
997.4	0.06	$H_2C=S$?	$\rho(CH_2)$	991.0
996.0				990.2[51]
994.9				
993.2				
954.6	0.24	$CH_3CH_2HC=C=O$	$\nu(C-C)$	1010
541.5	0.02	$CH_3CH_2HC=C=O$	$\delta oop (C-H)$	581

^{a} Tentatively assigned from B3LYP/aug-cc-pVTZ calculation. ^{b} Broadband with complex features (see Figure 6) with overlapped bands at 2147.8 (0.014), 2143.7 (0.06), 2135.4 (0.62), 2126.6 (0.47), and 2122.0 (0.47), relative intensities between parentheses.
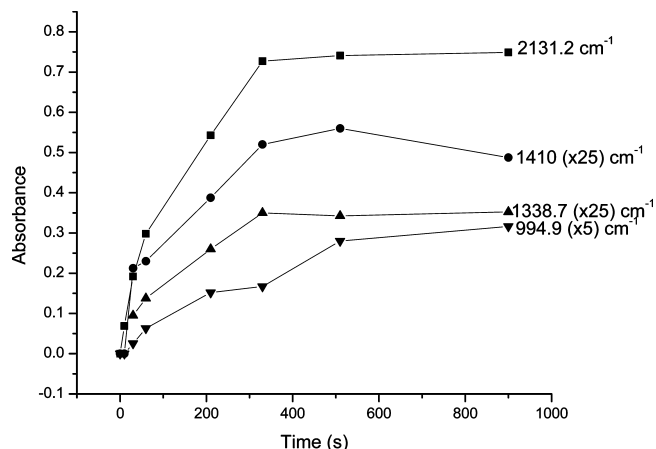
Figure 7. Plots as a function of the irradiation time of the intensities of selected bands tentatively assigned to ethyl ketene.

process, for which it is well-documented that decarbonylation is the main reaction channel in the gaseous phase.

In the case of the four-member related species β-propiothiolactone, also a ketene derivative, $CH_3HC=C=O$ was generated in the photolysis.[9] The elimination of a sulfur atom to give the corresponding ketene molecule is the dominant photodecomposition channel of the small-size β-propio- and γ-butyrothiolactones. Thus, it is plausible that excited states with characters mainly involving the −SC(O)− group play a central role in the photoevolution of these species. Indeed, the importance of this chromophore in the outermost valence electronic structure of both thiolactones has been confirmed through the analysis of its HeI photoelectron spectra.

The ring strain energy for γ-butyrothiolactone was estimated as 3.8 kcal mol^{-1} (G2MP2), a much lower value than that reported for β-propiothiolactone (16.4 kcal mol^{-1}, at the same level of calculation).[9] Thus, strain levels, at least in the ground electronic state, seem to play a minor role in determining the photochemical behavior of thiolactone species.

Supporting Information Available: Calculated geometric parameter, rotational constants (GHz) and dipole moment (D) for γ-butirothiolactone are given in Table S1. Liquid phase infrared and Raman spectra are given in Figure S1, and a plot as a function of irradiation time of the intensities of the bands assigned to $\nu_{as}(C=C=O)$ for ketene species is shown in Figure S2. Computed (B3LYP/aug-cc-pVTZ) frequencies for ketene species are given in Table S2. Table S3 lists the atomic charge computed [UB3LYP/6-311++G(d,p)] for the neutral and the low-lying cationic states of γ-butirothiolactone. This material is available free of charge via the Internet at http://pubs.acs.org.

References and Notes

(1) Bailey, W. J.; Bird, C. N. *J. Org. Chem.* **1977**, *42*, 3895.

(2) Noyce, D. S.; Banitt, E. H. *J. Org. Chem.* **1966**, *31*, 4043.

(3) Adam, W.; Baeza, J.; Liu, J.-C. *J. Am. Chem. Soc.* **1972**, *94*, 2000.

(4) Rai-Chaudhuri, A.; Chin, W. S.; Mok, C. Y.; Huang, H.-H. *J. Chem. Res. (S)* **1994**, 378.

(5) Rai-Chaudhuri, A.; Chin, W. S.; Kaur, D.; Mok, C. V.; Huang, H. H. *J. Chem. Soc. Perkin Trans. 2* **1993**, 1249.

(6) Li, Z.-H.; Wang, W.-N.; Fan, K.-N.; Wong, M. W.; Huang, H.-H.; Huang, W. *Chem. Phys. Lett.* **1999**, *305*, 474.

(7) Huang, H. H.; Fan, K. N.; Huang, W.; Li, Z. H.; Mok, C. Y.; Wang, W. N.; Chin, W. S. *Chem. Phys. Lett.* **1997**, *265*, 508.

(8) Chin, W. S.; Xu, Z. P.; Mok, C. Y.; Huang, H. H.; Mutoh, H.; Masuda, S. *J. Electron. Spectrosc. Relat. Phenom.* **1998**, *88−91*, 97.

(9) Dugarte, N. Y.; Erben, M. F.; Romano, R. M.; Boese, R.; Ge, M.-F.; Li, Y.; Della Védova, C. O. *J. Phys. Chem. A* **2009**, *113*, 3662.

(10) Huisgen, R. *Angew. Chem., Int. Ed.* **1986**, *25*, 297.

(11) NIST Mass Spec Data Center; Infrared Spectra. In *NIST Chemistry WebBook*; Linstrom, P. J. Mallard, W. G., Eds.; National Institute of Standards and Technology: Gaithersburg, MD; http://webbook.nist.gov.

(12) Geronés, M.; Erben, M. F.; Romano, R. M.; Della Védova, C. O.; Yao, L.; Ge, M. *J. Phys. Chem. A* **2008**, *112*, 2228.

(13) Zeng, X. Q.; Liu, F. Y.; Sun, Q.; Ge, M. F.; Zhang, J. P.; Ai, X. C.; Meng, L. P.; Zheng, S. J.; Wang, D. X. *Inorg. Chem.* **2004**, *43*, 4799.

(14) Frisch, M. J.; Trucks, G. W.; Schlegel, H. B.; Scuseria, G. E.; Robb, M. A.; Cheeseman, J. R.; Montgomery, J. A., Jr.; Vreven, T.; Kudin, K. N.; Burant, J. C.; Millam, J. M.; Iyengar, S. S.; Tomasi, J.; Barone, V.; Mennucci, B.; Cossi, M.; Scalmani, G.; Rega, N.; Petersson, G. A.; Nakatsuji, H.; Hada, M.; Ehara, M.; Toyota, K.; Fukuda, R.; Hasegawa, J.; Ishida, M.; Nakajima, T.; Honda, Y.; Kitao, O.; Nakai, H.; Klene, M.; Li, X.; Knox, J. E.; Hratchian, H. P.; Cross, J. B.; Adamo, C.; Jaramillo, J.; Gomperts, R.; Stratmann, R. E.; Yazyev, O.; Austin, A. J.; Cammi, R.; Pomelli, C.; Ochterski, J. W.; Ayala, P. Y.; Morokuma, K.; Voth, G. A.; Salvador, P.; Dannenberg, J. J.; Zakrzewski, V. G.; Dapprich, S.; Daniels, A. D.; Strain, M. C.; Farkas, O.; Malick, D. K.; Rabuck, A. D.; Raghavachari, K.; Foresman, J. B.; Ortiz, J. V.; Cui, Q.; Baboul, A. G.; Clifford, S.; Cioslowski, J.; Stefanov, B. B.; Liu, G.; Liashenko, A.; Piskorz, P.; Komaromi, I.; Martin, R. L.; Fox, D. J.; Keith, T.; Al-Laham, M. A.; Peng, C. Y.; Nanayakkara, A.; Challacombe, M.; Gill, P. M. W.; Johnson, B.; Chen, W.; Wong, M. W.; Gonzalez, C.; Pople, J. A. *Gaussian 03*; Revision B.04 ed.; Gaussian, Inc.: Pittsburgh PA, 2003.

(15) Cederbaum, L. S.; Schirmer, J.; Domcket, W.; von Niessen, W. *J. Phys. B* **1977**, *10*, L549.

(16) Cederbaum, L. S.; Domcke, W. *Adv. Chem. Phys.* **1977**, *36*, 205.

(17) Zhao, M.; Gimarc, B. M. *J. Phys. Chem.* **1993**, *97*, 4023.

(18) Ringer, A. L.; Magers, D. H. *J. Org. Chem.* **2007**, *72*, 2533.

(19) Curtiss, L. A.; Raghavachari, K.; Redfern, P. C.; Stefanov, B. B. *J. Chem. Phys.* **1998**, *108*, 692.

(20) Curtiss, L. A.; Raghavachari, K.; Pople, J. A. *J. Chem. Phys.* **1993**, *98*, 1293.

(21) Alonso, J. L. *J. Chem. Soc., Chem. Commun.* **1981**, *12*, 577.

(22) Harder, H.; Lesarri, A. G.; Alonso, J. L.; Dreizler, H. *Z. Naturforsch.* **1992**, *47A*, 588.

(23) Alonso, J. L.; Lopez, J. C.; Mata, F. *Z. Naturforsch.* **1981**, *37A*, 129.

(24) Zeiger, D. N.; Liebman, J. F. *J. Mol. Struct.* **2000**, *556*, 83.

(25) Bach, R. D.; Dmitrenko, O. *J. Am. Chem. Soc.* **2006**, *128*, 4598.

(26) Pitzer, K. S.; Donath, W. E. *J. Am. Chem. Soc.* **1959**, *81*, 3213.

(27) Wiberg, K. B.; Bonneville, G.; Dempsey, R. *Isr. J. Chem.* **1983**, *23*, 85.

(28) Johnson, R. P.; Daoust, K. J. *J. Am. Chem. Soc.* **1995**, *117*, 362.

(29) Daoust, K. J.; Hernandez, S. M.; Konrad, K. M.; Mackie, I. D.; Winstanley, J.; Johnson, R. P. *J. Org. Chem.* **2006**, *71*, 5708.

(30) Stirling, C. J. M. *Tetrahedron* **1985**, *41*, 1613.

(31) Bachrach, S. M. *J. Org. Chem.* **2008**, *73*, 2466.

(32) Kenneth, B. W. *Angew. Chem., Int. Ed.* **1986**, *25*, 312.

(33) Saiyasombat, W.; Molloy, R.; Nicholson, T. M.; Johnson, A. F.; Ward, I. M.; Poshyachinda, S. *Polymer* **1998**, *39*, 5581.

(34) Della Védova, C. O.; Romano, R. M.; Oberhammer, H. *J. Org. Chem.* **2004**, *69*, 5395.

(35) Nagy, P. I.; Tejada, F. R.; Sarver, J. G.; Messer, W. S., Jr. *J. Phys. Chem. A* **2004**, *108*, 10173.

(36) El-Assar, A. M. M.; Nash, C. P.; Ingraham, L. L. *Biochemistry* **1982**, *21*, 1972.

(37) Hilal, R.; El-Aaser, A. M. *Biophys. Chem.* **1985**, *22*, 145.

(38) Jinno, M.; Watanabe, I.; Yokoyama, Y.; Ikeda, S. *Bull. Chem. Soc. Jpn.* **1977**, *50*, 597.

(39) Pan, J. F.; Huang, W.; Chin, W. S.; Huang, H. H.; Mok, C. Y. *J. Electron Spectrosc. Relat. Phenom.* **1998**, *88−91*, 91.

(40) Geronés, M.; Downs, A. J.; Erben, M. F.; Ge, M.; Romano, R. M.; Yao, L.; Della Védova, C. O. *J. Phys. Chem. A* **2008**, *112*, 5947.

(41) (a) Erben, M. F.; Della Védova, C. O. *Inorg. Chem.* **2002**, *41*, 3740. (b) Erben, M. F.; Della Védova, C. O. *Helv. Chim. Acta* **2003**, *86*, 2379.

(42) Nagata, S.; Yamabe, T.; Fukui, K. *J. Phys. Chem.* **1975**, *79*, 2335.

(43) Price, W. C. Ultraviolet Photoelectron Spectroscopy: Basic Concepts and the Spectra of Small Molecules. In *Electron Spectroscopy: Theory and Applications*; Brundle, C. R., Baker, A. D., Eds.; Academic Press: New York, 1977; Vol. 1; p 151.

(44) Lere-Porte, J. P.; Galsomias, J.; Petrissans, J. *C. R. Acad. Sci.* **1984**, *299 II*, 159.

(45) Seth-Paul, W. A. *J. Mol. Struct.* **1969**, *3*, 403.

(46) (a) Herzberg, G. *Molecular Spectra and Molecular Structure II: Infrared and Raman Spectra of Polyatomic Molecules*; Van Nostrand: New York, 1945. For examples, see(b) Torrico-Vallejos, S.; Erben, M. F.; Ge, M.-F.; Willner, H.; Della Védova, C. O. *J. Phys. Chem. A* **2010**, *114*, 3703. (c) Erben, M. F.; Padró, J. M.; Willner, H.; Della Védova, C. O. *J. Phys. Chem. A* **2009**, *113*, 13029.

(47) Romano, R. M.; Della Védova, C. O.; Downs, A. J. *J. Phys. Chem. A* **2002**, *106*, 7235.

(48) Moore, C. B.; George, C. P. *J. Chem. Phys.* **1963**, *38*, 2816.

(49) Harrison, J. A.; Frei, H. *J. Phys. Chem.* **1994**, *98*, 12142.

(50) Johnston, D. E.; Sodeau, J. R. *J. Chem. Soc. Faraday Trans.* **1992**, *88*, 409.

(51) Clouthier, D. J.; Ramsay, D. A. *Annu. Rev. Phys. Chem.* **1983**, *34*, 31.

(52) Winter, P. R.; Rowland, B.; Hess, W. P.; Radziszewski, J. G.; Nimlos, M. R.; Ellison, G. B. *J. Phys. Chem. A* **1998**, *102*, 3238.

(53) Hawkins, M.; Almond, M. J.; Downs, A. J. *J. Phys. Chem.* **1985**, *89*, 3326.

(54) Romano, R. M.; Della Védova, C. O.; Downs, A. J. *J. Phys. Chem. A* **2004**, *108*, 7179.